Geochemistry, Geophysics, Geosystems

RESEARCH ARTICLE
10.1029/2021GC009662

Key Points:

- The Pāpaku fault shows a ≥160 m thick damage zone as defined by fracture density within a drillcore from IODP Exp. 375
- Damage is asymmetric around the thrust fault, with a wider and more intensely fractured damage zone in the hanging wall than the footwall
- Damage decay and damage zone thickness of subduction faults are similar to continental faults

Supporting Information:

Supporting Information may be found in the online version of this article.

Correspondence to:

H. M. Savage,
hsavage@ucsc.edu

Citation:

Savage, H. M., Shreedharan, S., Fagereng, Å., Morgan, J. K., Meneghini, F., Wang, M., et al. (2021). Asymmetric brittle deformation at the Pāpaku fault, Hikurangi subduction margin, NZ, IODP Expedition 375. *Geochemistry, Geophysics, Geosystems*, *22*, e2021GC009662. https://doi.org/10.1029/2021GC009662

Received 19 JAN 2021
Accepted 2 AUG 2021

Asymmetric Brittle Deformation at the Pāpaku Fault, Hikurangi Subduction Margin, NZ, IODP Expedition 375

Heather M. Savage[1], Srisharan Shreedharan[2,9], Åke Fagereng[3], Julia K. Morgan[4], Francesca Meneghini[5], Maomao Wang[6], David D. McNamara[7], Laura M. Wallace[8,9], Demian M. Saffer[2,9], Philip M. Barnes[10], Katerina E. Petronotis[11], and Leah J. LeVay[11]

[1]Department of Earth and Planetary Sciences, University of California, Santa Cruz, CA, USA, [2]Department of Geosciences, The Pennsylvania University, University Park, PA, USA, [3]School of Earth & Ocean Sciences, Cardiff University, Cardiff, UK, [4]Department of Earth Sciences, Rice University, Houston, TX, USA, [5]Dipartimento di Scienze della Terra, Universita degli Studi di Pisa, Pisa, Italy, [6]College of Oceanography, Hohai University, Nanjing, China, [7]Department of Earth, Ocean and Ecological Sciences, University of Liverpool, Liverpool, UK, [8]GNS Science, Lower Hutt, New Zealand, [9]University of Texas Institute for Geophysics, Austin, TX, USA, [10]National Institute of Water and Atmospheric Research, Wellington, New Zealand, [11]International Ocean Discovery Program, Texas A&M University, College Station, TX, USA

Abstract Quantifying fault damage zones provides a window into stress distribution and rheology around faults. International Ocean Discovery Program (IODP) Expeditions 372/375 drilled an active thrust splay fault within the Hikurangi subduction margin. The fault, which is hosted in Pleistocene clastic sediments, is surrounded by brittle fractures and faults as well as ductile deformation features. We find that fracture density in the damage zone enveloping the fault is asymmetric, with the hanging wall showing greater overall fracture density and at greater distances from the fault than the footwall. Furthermore, the peak in fracture density occurs within an area of mesoscale folding and localized slip in the hanging wall rather than adjacent to the main fault zone. We attribute the asymmetry in damage to disparate deformation histories between the hanging wall and footwall, greater ductile deformation within the footwall, and/or dynamic stress asymmetry around a propagating rupture. Damage asymmetry is common at shallow depths in subduction zones and influences the mechanical and hydrological properties of the fault, such as channelized fluid flow and fault stability. Finally, we demonstrate that subduction zone faults show similar damage-displacement scaling as continental faults.

Plain Language Summary Fault damage zones form when slip along faults creates off-fault stresses that bring the surrounding rock to failure. The greatest fracturing usually occurs closest to the fault core. During fault zone drilling of Hikurangi subduction zone east of New Zealand, we found that damage around a large splay fault is asymmetric, and the peak in fracture density occurs ~25 m above the fault, rather than adjacent to the fault core. We hypothesize that this is caused by folding and fracturing in the hanging wall, more ductile deformation in the footwall, and/or a stress asymmetry around the fault that was created while the fault was slipping.

1. Introduction

Most large-displacement faults consist of a core of comminuted rock hosting localized slip surrounded by a halo of fractures that has greater fracture density than the undeformed rocks outside of the fault, known as the damage zone (Caine et al., 1996). Fault damage zones form from stresses associated with fault slip such as fracture tip propagation, fault-related folding, frictional variations along the fault or propagating rupture, accommodation around geometric irregularities and roughness, and shaking associated with seismic waves (Brune 2001; Caine et al., 1996; Chester & Logan, 1986; Mitchell et al., 2011; Savage & Brodsky, 2011; Savage & Cooke, 2010; Tavani et al., 2015; Vermilye & Scholz, 1998). The damage zone is mechanically different from the surrounding host rock, having lower elastic wavespeed (Cochran et al., 2009; Y.-G. Li et al., 2001) and generally greater permeability (Mitchell & Faulkner, 2008). These differences in material properties play a role in the thermo-hydro-mechanical coupling between the damage zone and the host rock. For instance, preferential fluid flow through damage zones can transport heat and solutes, as well as influence slip on

the fault interface (Saffer, 2015) and control the spatial distribution of foreshocks and aftershocks (Savage et al., 2017). Fault damage can also cause significant changes in rupture propagation direction and velocity due to the energy sink from slip along fractures (Bhat et al., 2010), as well as potentially slow propagating ruptures and promote tsunami earthquakes or other slower slip phenomena (e.g. Kanamori & Kikuchi, 1993).

Damage zones grow progressively with increasing total fault displacement (Chester & Logan, 1986; Mitchell & Faulkner, 2009; Savage & Brodsky, 2011). However, most of our current understanding of damage zone morphology is based on continental faults. Drillcores acquired from active, shallow subduction zone decollements and splay faults often qualitatively show asymmetric damage zones, where the hanging wall is relatively more fractured over greater thickness than the footwall (McNeill et al., 2004; Morgan et al., 2007; Saffer, 2015; Tobin et al., 2001). However, only one subduction damage zone, the Japan Trench, has been investigated quantitatively in terms of fracture density (Keren & Kirkpatrick, 2016).

IODP Expedition 372/375 drilled through the Pāpaku fault at Site U1518 near the front of the accretionary prism of the Hikurangi subduction margin, New Zealand (Saffer et al., 2019; Wallace et al., 2019) (Figure 1). This kilometer-scale thrust fault splays upward from the plate interface, which displays a range of slow slip behavior (Bell et al., 2014; Shaddox & Schwartz, 2019; Todd et al., 2018; Wallace et al., 2016). Although SSEs within the area are usually modeled as occurring on the megathrust, some component of the slow slip could branch upwards along the Pāpaku fault, consistent with recent observations on more landward accretionary prism faults (Shaddox & Schwartz, 2019). Furthermore, biomarker thermal maturity anomalies within the Pāpaku fault indicate high frictional temperatures only achievable during earthquake rupture have occurred along this part of the fault in the past (Coffey et al., 2021; Rabinowitz et al., 2017; Savage et al., 2018). Initial results from drilling showed a mix of brittle and ductile structural features within the Pāpaku fault zone, which has been interpreted as possible evidence for a range of slip speeds or effective stresses (Fagereng et al., 2019). Here, we analyze the brittle damage zone surrounding the Pāpaku fault by quantifying fracture density within the drillcore. As observed in other active shallow thrusts in subduction zones and continental faults (Brune, 2001; Heermance et al., 2003; Morgan et al., 2007; Saffer, 2015; Tobin et al., 2001), we show that fracture density is asymmetric around the fault, with a wider, more fractured damage zone in the hanging wall and a narrow footwall damage zone that displays a mix of brittle/ductile deformation. We discuss how damage asymmetry might form and how brittle deformation in subduction zones compares to continental faults.

2. Pāpaku Fault, IODP Site U1518

The Pacific plate subducts beneath the Australian plate along the Hikurangi Trough at a rate of ~52 mm/yr in the drilling transect area (Wallace et al., 2004). The Pāpaku fault is a large thrust splay fault (Barker et al., 2018) with approximately 6 km of displacement (Barnes et al., 2020; Fagereng et al., 2019), making it one of the major active structures accommodating shortening within the accretionary wedge. The fault is currently undergoing E-W convergence (McNamara et al., 2021) and thrusts Early-Middle Pleistocene hemipelagic, silty mudstone and silty turbidite sequences over Middle-Late Pleistocene hemipelagic silts and muds (Wallace et al., 2019). Because these stratigraphic units are compositionally similar, there is little lithologic contrast across the fault at shallow depths. There are, however, differences in consolidation and deformation states (see below). The hanging wall contains folds at multiple scales (including a km-scale, open, moderately inclined, fault-bend fold), smaller faults, and abundant fractures (Fagereng et al., 2019; McNamara et al., 2021). Mesoscale folding was inferred from changes in dip angle within the hanging wall, which generally vary between ~0 and 45° and dip to the south-southwest, consistent with the style of the km-scale fold. In one case a small, recumbent fold hinge was recovered with clear increase in fracturing in the hinge zone suggesting tighter folds occur at the mesoscale (Fagereng et al., 2019; Wallace et al., 2019). Otherwise, gaps in core recovery made it difficult to characterize fold geometry or style.

At Hole U1518F the top of the fault was defined at 304 mbsf by both a structural transition (fractured and folded but coherent bedding to disrupted fault rocks), and a biostratigraphically defined age inversion of ~0.5 My (Fagereng et al., 2019; Wallace et al., 2019). The fault core contains breccias and zones of ductile features such as flow banding (Fagereng et al., 2019). Locally, ductile structures are overprinted by filled fractures, indicating that both deformation styles pre-date drilling. Both brittle and ductile deformation

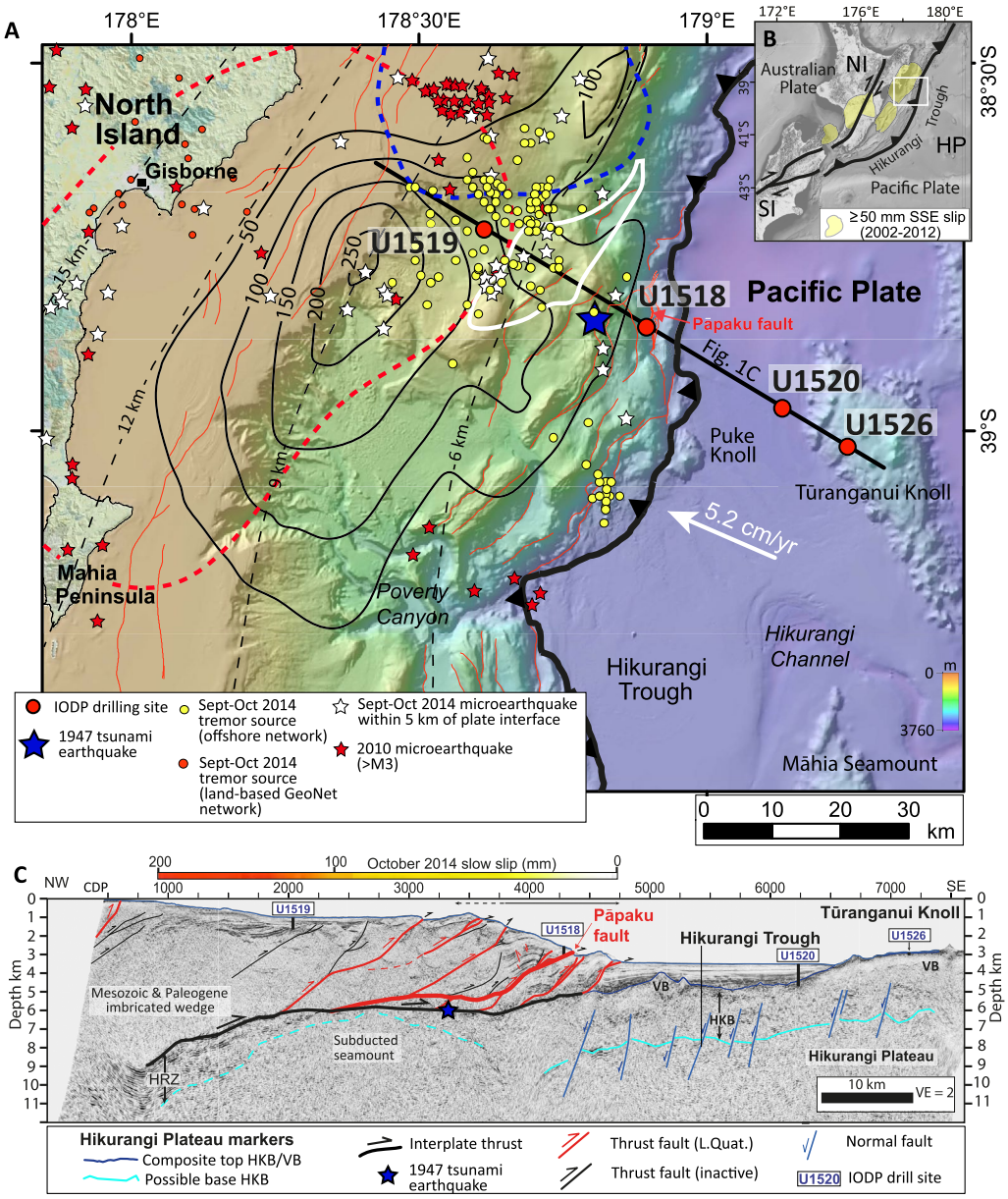

Figure 1. Adapted from Barnes et al. (2020). (a) Bathymetric map of eastern coast of the North Island, NZ. Expedition 372/375 drilling sites are shown with the red dots. Red dashed, blue dashed and solid black contour lines show recent slow slip patches from 2010 and 2014. Black dashed contours show approximate depth to the plate interface. (b) Map of the North Island, NZ. White box outlines area in (a). (c) Cross-section of the accretionary wedge. IODP Hole U1518F intersected the fault at a depth of 304 mbsf. A kilometer-scale antiform is visible in the hanging wall of the fault.

decrease in intensity below the base of the fault at 322 mbsf. At 351–361 mbsf, a subsidiary fault has been interpreted from an increase in prevalence of both brittle and ductile deformation features (Fagereng et al., 2019; Wallace et al., 2019). No age inversion is seen at the subsidiary fault, below which the rocks are still locally fractured but relatively undeformed.

3. Methods

We analyze core from Hole U1518F collected below 198 mbsf using a rotary core barrel bottom hole assembly (Wallace et al., 2019). From the seafloor to 198 mbsf, drilling disturbance in core from Hole U1518E made it impossible to analyze fractures. We counted fractures along high-resolution core photos taken immediately

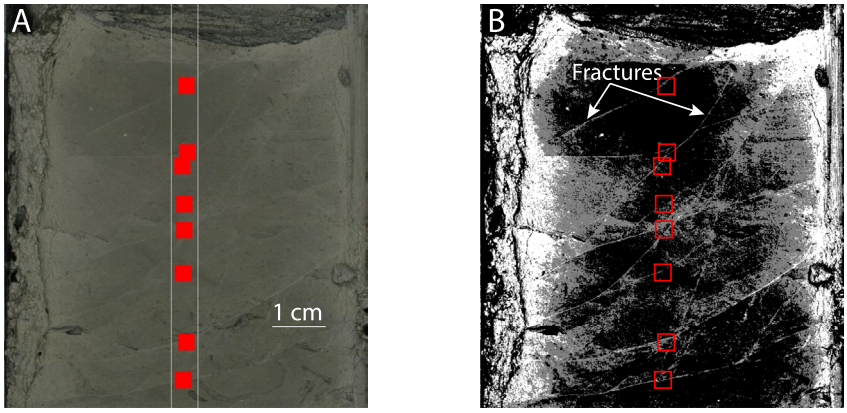

Figure 2. Core Section U1518F-9R-4 (56.3–63.8 cm), 268.82–268.90 mbsf. (a) High-resolution core photograph. Fracture picks (red squares) within 0.5 cm of the drillcore center (gray vertical lines). Only filled fractures are counted. (b) Gray-scale, contrast-boosted image of (a). Filled fractures stand out as white against a dark gray/black background.

after the drillcore was split (Figure 2a). The sediments within the drillcore contained both open fractures and fractures filled with white material that is mostly clay (Fagereng et al., 2019). We cannot unambiguously establish whether the open fractures were induced by drilling, whereas the filled fractures cannot be related to drilling-induced damage as the clay would have taken some time to form within the cracks. We therefore limit our analysis to the filled fractures. Keren and Kirkpatrick (2016) similarly separated out drilling-induced versus natural fractures in their analysis, and Fagereng et al. (2019) provide further discussion on separating seafloor and drilling-induced deformation features in the U1518 drillcores. Limiting our analysis in this way means that we might undercount younger fractures, fractures that experience higher velocity fluid flow, and/or fractures where fluids are not supersaturated (El Mountassir et al., 2014; Skelton et al., 2014). However, limiting the data set to tectonic fractures is a more conservative approach and has been shown to not have a large effect on damage decay or damage zone thickness measurements at another site (Keren & Kirkpatrick, 2016).

In order to make the filled fractures visually prominent, we converted the image to gray scale and boosted the contrast (Figure 2b). This ensured that the filled fractures were brighter and the open (potentially drilling induced) fractures became darker. We measured a vertical, linear transect through the center of the core and counted fractures within 0.5 cm (±0.25 cm) of the centerline (Figure 2a). The depth along the core was collected with the associated fracture. Core recovery was incomplete throughout the area of interest, with average recovery of ~43% throughout the hole, and recovery of ~37% within the fault zone (Wallace et al., 2019). Within each 10 m cored interval (the stroke of the coring assembly), the entire recovered core was pushed to the top of the core liner and then divided into shorter sections (Wallace et al., 2019). Because of the uncertainty in fracture spacing and precise position caused by this procedure, we calculated an average fracture density for each section of core by dividing the number of fractures in each section by the section length (up to ~1.5 m). Each point on a fracture density plot is therefore a binned value for a section plotted at the depth below seafloor to the top of that section. Using an average value addresses the possibility that a section may consist of pieces that were not initially adjacent before the core was pushed to the top of the liner, however it does not address if the section is in its original place within the total 10 m drive for the core. The location of each fracture, along with the core image analysis code, is available in the supporting information. Logging-while-drilling (LWD) image logs from Hole U1518B revealed some areas of faulting and fracturing (Wallace et al., 2019), including both conductive and resistive fractures (Cook et al., 2020), at similar depths as discussed here.

4. Fault Damage Zone Properties

4.1. Fracture Density and Physical Properties

We analyze the damage zone in the context of the lithology and material properties of the fault (Figure 3). Fracture density generally increases in the vicinity of the main fault (to a maximum of 111 fractures/m),

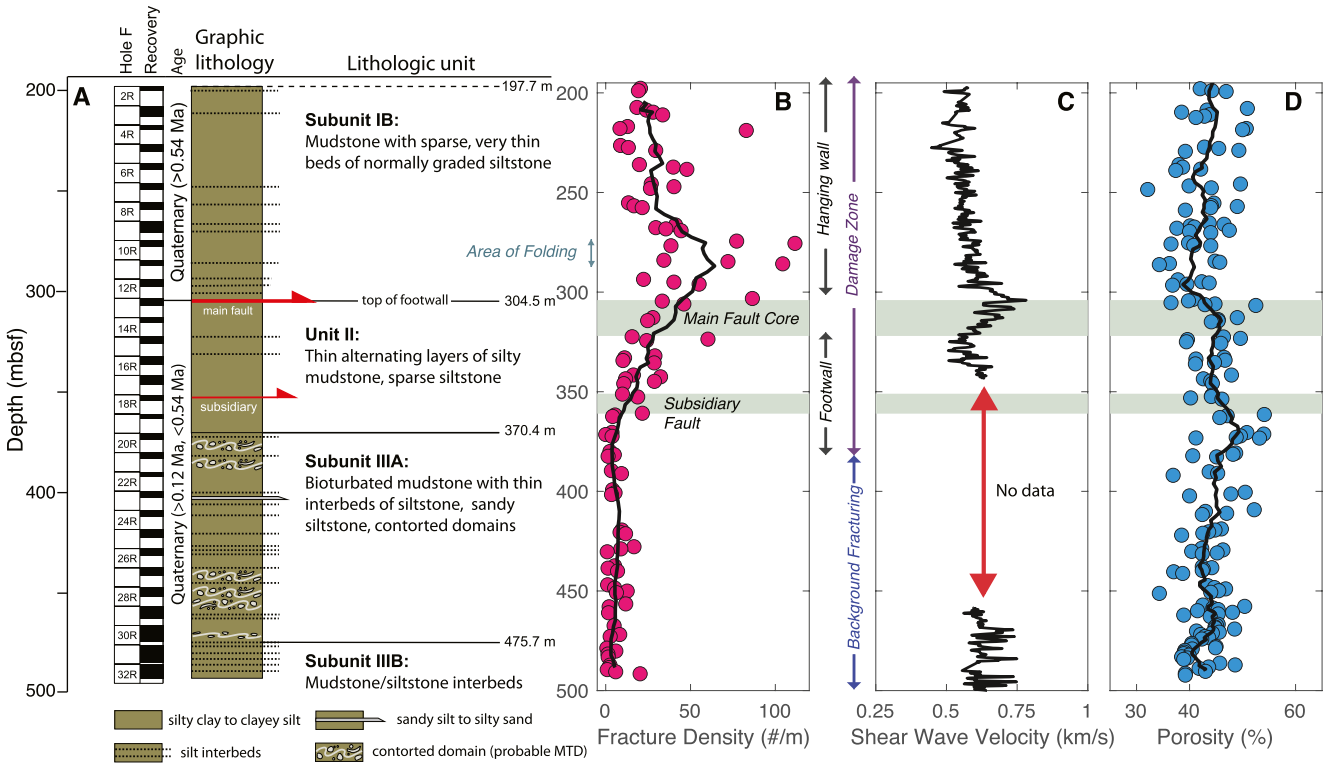

Figure 3. (a) Core description and recovery for Hole U1518F (Wallace et al., 2019). Recovered portions of the core are shown in black and missing sections in white. Lithology consists of predominantly hemi-pelagic silty muds/mudstones and turbidites. MTD, mass transport deposit. (b) Fracture density as a function of depth. Each pink dot represents the number of fractures per meter for each section of core (core lengths are up to 1.5 m). Black line shows the 10-point moving average. (c) Logging-while-drilling (U1518B) measurements show that shear velocity increases in the hanging wall with depth and decreases throughout the fault core and into the footwall (Wallace et al., 2019). (d) Shipboard measurements of porosity slightly decrease throughout the core, with an uptick at the top of the main fault and below the subsidiary fault at ~375 mbsf (Wallace et al., 2019). Porosity is calculated from the shipboard moisture and density (MAD) measurements as the ratio of fluid volume to wet sample volume. Errors in local porosity measurements are smaller than the size of the circles. Black lines show the 10-point moving average.

and damage is asymmetric around the fault (Figure 3b). The hanging wall has substantially higher fracture density than the footwall. Unlike most fault zones (e.g. Keren & Kirkpatrick, 2016; Savage & Brodsky, 2011), the peak in fracture density does not occur closest to the main fault but in the hanging wall around 275–286 mbsf, in an area of mesoscopic folding observed in the core 20–30 m above the main fault (French & Morgan, 2020; Wallace et al., 2019). Although values are scattered, average fracture density generally decreases with depth from this peak, down to the base of the subsidiary fault at 361 mbsf. Below the subsidiary fault, the fracture density decays slightly with depth to 392 mbsf, below which it is fairly constant at ~1–10 fractures/m, which we define as the background fracture density for the footwall. The hanging wall fracturing never reaches a background, as the fracture density is still decreasing with decreasing depth at the top of the core.

For comparison with physical properties, Figures 3c and 3d show shear wave velocity and porosity measurements at Site U1518 (Cook et al., 2020; Wallace et al., 2019). The shear wave velocity is higher in the hanging wall near the fault and decreases through the fault zone core into the footwall, showing that although the lithology is similar across the fault, there is a compliance contrast. We note that the shear wave velocity was calculated from data measured in Hole U1518B, where the top of the Pāpaku fault is identified from logging data to be ~11 m deeper than in Hole U1518F (Cook et al., 2020). This means that shear wave velocity may start to decrease several meters above rather than within the fault, but the shear wave velocity is still generally higher in the hanging wall than the fault and footwall. The porosity decreases slightly through the hanging wall, slightly increases within the main fault zone, and more markedly increases below the subsidiary fault. From about 375 mbsf, porosity decreases with depth to the bottom of the core.

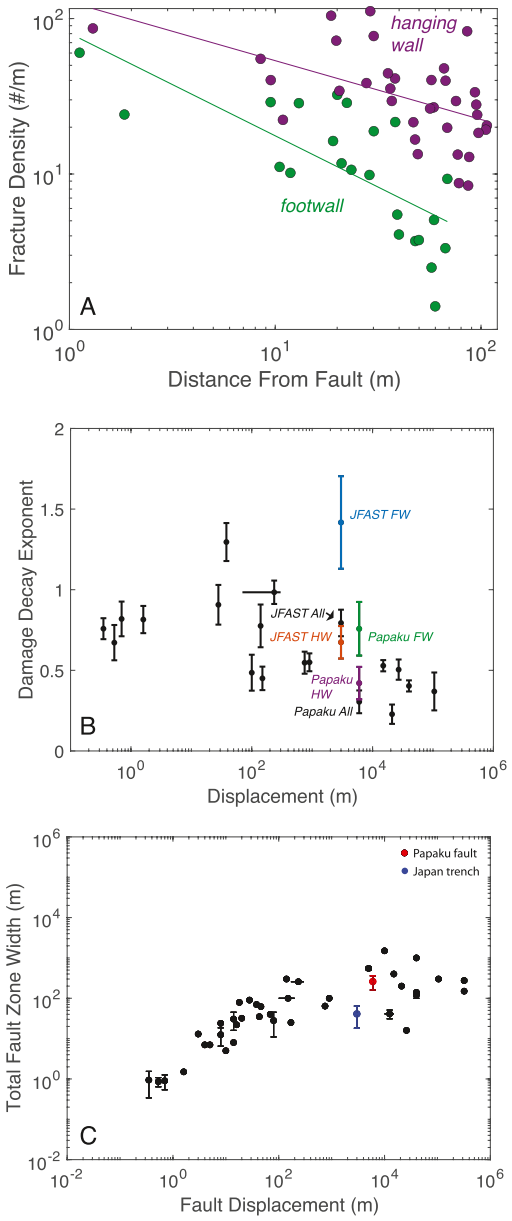

Figure 4. (a) Fracture density decay within the Pāpaku fault hanging wall (purple) and footwall (green). The falloff in fracture density is steeper within the footwall. (b) Compilation of fracture density decay exponent as a function of fault displacement for JFAST, Pāpaku fault, and continental faults. Uncertainty bars represent the mean absolute deviation of the damage decay exponent, n, from bootstrapping on 10,000 realizations. Each realization randomly samples distance/density pairs with replacement and reflects the effect of sampling uncertainty on the decay exponent. (c) Total fault zone with as a function of displacement. Data from (b and c) are from Keren and Kirkpatrick (2016) and Savage and Brodsky (2011).

The difference in consolidation history as reflected in porosity contrast between the hanging wall and footwall has been suggested as a reason for the more brittle behavior of the hanging wall (Fagereng et al., 2019; French & Morgan, 2020).

4.2. Damage Density Decay and Width

The spatial decay in damage provides insight into how stress decays with distance from the fault, integrated over its entire tectonic history. To quantify the damage decay exponent, we fit a power law to the hanging wall and footwall data as a function of distance from the fault (Savage & Brodsky, 2011):

$$d = cx^{-n} \quad (1)$$

where d is number of fractures, x is distance from the fault, n is the exponent, and c is a constant. To compare with similar studies, we only include the fractures outside of the main fault core at 304.5–322 mbsf (Keren & Kirkpatrick, 2016; Mitchell & Faulkner, 2009; Savage & Brodsky, 2011). For the footwall rocks, we fit the fracture density decay from 322-392 mbsf. Below this depth there is a relatively constant fracture density to the bottom of the core, so we consider this the background fracture density of the footwall (Figure 3b). However, we consider the entire hanging wall from 198 to 304.5 mbsf because fracture densities continually decrease with distance from the fault without achieving a uniform background. The footwall decay is sharp compared to the hanging wall, with decay exponents of $n = 0.76$ (± 0.17) and $n = 0.42$ (± 0.1), respectively (Figure 4a). The occurrence of the peak in fracture density 20–30 m above the fault reduces the decay exponent in the hanging wall. However, if the data from both sides of the Pāpaku fault are fit by a single curve, the average decay is similar to that of the hanging wall (Figure 4b). This is because the greater number of fractures in the hanging wall dominates the signal.

The damage zone decay exponents, n, for the Pāpaku fault are similar to continental fault zones with comparable displacement (Figure 4b), whereas the decay exponent at the Japan trench decollement footwall is much larger than other faults of similar size (Keren & Kirkpatrick, 2016). However, the asymmetry between the highly fractured hanging wall damage with gentle density decay over the narrower, steeply decaying footwall damage is similar at the Japan trench decollement and Pāpaku fault (Figure 4b). When the fracture densities from the Japan trench are collapsed into a single data set, the damage decay is similar to other faults with the same displacement (Figure 4b).

The total damage zone thickness, defined by the depth range where the fracture density is above the background, is at least 160 m, with the caveat that the hanging wall damage could extend above 200 mbsf as the hanging wall fractures do not reach a background state in the interval we measured. A total fault zone thickness of at least 160 m is consistent with the average fault thickness reported for other subduction zone splays and megathrusts (100–350 m; Rowe et al., 2013; Figure 4c). An upper limit of 360 m thickness includes the entire hanging wall to the sea floor, as we cannot rule this out due to disturbance within the cores above ~200 mbsf, but would still be in line with fault thicknesses measured in other subduction zones and continental faults.

5. Discussion and Implication

5.1. Evolution of Damage Zone Asymmetry

Hanging wall and footwall damage around the Pāpaku fault contrasts in width, fracture decay, and peak fracture density, with the hanging wall damage zone being wider, more fractured, and with a smaller decay exponent. There are several possible reasons for the sustained damage asymmetry at shallow subduction faults and other faulting environments that may have important consequences for slip.

5.1.1. Deformation History

The hanging wall has a longer deformation and stress history than the footwall, including experiencing greater total fault displacement. This, along with greater consolidation of more deeply buried hanging wall rocks, could lead to the greater overall fracture density seen in the hanging wall (French & Morgan, 2020). However, damage zone thickness tends to saturate after a fault has experienced ∼100 m of displacement (Figure 4c; Savage & Brodsky, 2011). Because both sides of the Pāpaku fault have experienced at least this much displacement, we think it is unlikely that the damage asymmetry is solely related to the different total slip that either side of the fault has experienced.

5.1.2. Influence of Folding

The fault-related folding within the hanging wall has likely enhanced damage zone fracturing as well. Fracturing occurs on folds where curvature is greatest, such as at the fold hinge, and decreases with distance to the neutral surface within a folded layer (e.g. Tavani et al., 2015). However, the bending stresses can be modulated by friction between interlayers, friction of the underlying fault, fault dip, and mechanical stratigraphy of the strata, with low friction and thinner/weaker mechanical layers having lower fracture density (Ju et al., 2014; Savage et al., 2010). In the relatively uniform lithostratigraphic sequence in the hanging wall (Figure 3a), there are no massive mechanical layers that would be more likely to fracture than surrounding layers. Furthermore, folding models that include fault-related stresses show that the fault stresses dominate fracture patterns close to the fault (Y. Li et al., 2018). Therefore, it is unclear if fold-related fracturing would necessarily decrease with distance from the fault, although the fold-related fracturing could widen the damage zone. Structural position along the fold can also influence fracturing, but due to the position of Site U1518 relative to a km-scale hanging wall antiform observed in seismic data it is likely that we are sampling a single structural position of the fold (rather than comparing disparate parts of the fold such as hinge vs. limb). We can expect that layers of the large-scale fold have similar deformation histories, however, we cannot fully discount the influence of local, parasitic folding that are not resolved in seismic data.

5.1.3. Earthquake Rupture

Dynamic stresses during earthquake slip can impart stress asymmetry around a seismically active fault and give rise to persistent differences in damage zone thickness and decay. The Pāpaku fault shows evidence that earthquake slip has occurred at Site U1518 (Coffey et al., 2021). A propagating rupture can produce asymmetric damage, and depending on the fault geometry relative to the stress orientation, that damage can occur on either the compressive or extensive quadrant (Andrews & Ben-Zion, 1997; DeDontney et al., 2011; Duan, 2008; Ma & Beroza, 2008; Templeton & Rice, 2008; Viesca et al., 2008). Because we have sampled a very shallow portion of the fault, it is most likely that any propagating rupture would come from depth, meaning that the hanging wall would be in the compressive quadrant of a propagating rupture. For the compressive quadrant to experience more stress and plastic strain than the extensive quadrant, the most compressive stress would need to be at a low angle to the dip of the fault (Templeton & Rice, 2008), which is the case here (McNamara et al., 2021). Furthermore, an undrained, poroelastic response to the rupture tip stresses would further weaken the hanging wall and strengthen the footwall, amplifying the asymmetric damage (Viesca et al., 2008).

Finally, although lithology is similar across the shallow reaches of the Pāpaku fault at Site U1518, the shear wave speed and porosity differences (due to different consolidation and lithification history) between the hanging wall and footwall (Figures 3c and 3d) give rise to a compliance contrast that would create an asymmetric stress concentration at the tip of a propagating slip patch, with a wider zone of high stress in the

stiffer material (Duan, 2008). This could create a wider damage zone in the hanging wall, which is stronger than the footwall in triaxial experiments at in situ conditions (French & Morgan, 2020).

5.1.4. Brittle Versus Ductile Deformation

The difference in deformation style between the hanging wall and footwall (brittle vs. brittle-ductile) should also contribute to the damage asymmetry. The weaker, more porous footwall exhibits greater ductile deformation, and has a sharper decay in fractures with distance from the fault. Whereas the hanging wall is likely to fracture over a range of fault slip behaviors (Fagereng et al., 2019), the footwall might fracture only at higher strain rates, such as during earthquake slip, or from increase in pore pressure. For instance, the subsidiary fault in the footwall shows little additional fracturing at its location whereas the peak in fracture density in the entire fault zone occurs within an area of small localized slip zones and folding in the hanging wall (Figure 3b). Significant ductile deformation in the main fault zone and footwall could also erase earlier fracturing (Fagereng et al., 2019).

5.1.5. Fracture Healing

Faults may not accumulate damage inexorably over time. Damage asymmetry seen in shallow subduction regions like at the Pāpaku fault may not continue with depth. For example, out-of-sequence thrusts exhumed from sub-greenschist conditions tend to show wider footwall damage, possibly due to the hanging wall experiencing more fracture healing at higher temperatures (Hamahashi et al., 2013; Rowe et al., 2009). Furthermore, damage zones may heal more completely on both sides of the fault if ambient temperature is high enough (Williams et al., 2016), or fractures on both sides are effectively healed by fault-related cementation (Kristensen et al., 2016). Therefore, the asymmetry may be a shallow feature down to a depth controlled by the onset of efficient healing, which in subduction zones is promoted by a range of temperature-dependent diagenetic process occurring at 100–150°C (e.g. Moore & Saffer, 2001). Damage zones are often emphasized as places where elastic moduli and permeability systematically change with increased deformation (e.g. Blake & Faulkner, 2016), but it is important to keep in mind that fracture healing, including clay filling as seen at the Pāpaku fault, means that the most fractured material in a damage zone may not be the most hydraulically conductive or mechanically compliant.

5.2. Evolution of Fault Width and Damage Decay With Displacement

The processes that can create and heal damage as discussed above have been documented in other fault zones and here we compare how damage zones in different faulting environments evolve over total displacement. Savage and Brodsky (2011) demonstrated that continental fault zone width saturates after about 150 m in total displacement at widths of 0.1–1 km. Large-displacement subduction faults show similar saturation in total width (Keren & Kirkpatrick, 2016; Rowe et al., 2013), indicating a similar thickness in plastic yielding for different fault types. Interestingly, this consistency in total thickness is maintained despite damage zone asymmetry. The upper cutoff in damage zones thickness has been attributed to the limiting effect of the seismogenic zone depth on stress concentration at the rupture front (Ampuero & Mao, 2017). Recent work has suggested that fault core thickness also scales with displacement and has a similar saturation point after around 150 m of total displacement (McKay et al., 2021); however, the authors attribute the change in scaling to difference in growth between intra- and interplate faults. For now, it is difficult to distinguish which scenario is correct, as the intraplate faults generally have less displacement and the interplate faults generally have more. If like damage zones, the fault core scales with seismogenic zone width, this could relate fault core formation back to rupture tip stresses.

The damage decay exponent also appears to have similar scaling with displacement for both continental and subduction-related faults (Figure 4b). When considered separately, the subduction faults show a large difference in damage decay between footwall and hanging wall, and indeed the footwall for the Japan trench has a much steeper decay than other faults with equivalent displacement. However, when the data from both sides are fit with a single curve, the decay is similar to continental faults with similar displacements. As the majority of the faults in the data set similarly combine the hanging wall and footwall, this is the more appropriate comparison. Much of our current understanding of damage zones is based on continental faults, with little data available from faults in subduction zones for comparison. We also note

that the continental fault compilation is dominated by normal faults hosted in sedimentary rock, and a more complete picture of continental and subduction faults may be necessary for a better comparison.

6. Conclusions

The Pāpaku fault, a thrust splay in the frontal wedge of the Hikurangi subduction zone is represented by an 18-m thick recovered brittle-ductile main fault enveloped by a ≥160 m wide damage zone. Damage is asymmetric, where the hanging wall damage zone is wider and more fractured than the footwall. We hypothesize that the asymmetry is caused by different consolidation and deformation histories across the fault, a mixture of brittle and ductile deformation styles, and/or asymmetric stress during earthquake ruptures. Damage asymmetry is likely common at shallow depth in subduction zones, as large across-fault contrasts in deformation history and compliance will typically arise from underthrusting and/or subduction of unconsolidated sediments beneath a more lithified accretionary wedge. Finally, we show that subduction and continental fault zone thickness and damage decay have similar scaling as a function of displacement, and that both fault thickness and damage decay saturate after ~100 m to 1 km of displacement in both settings.

Data Availability Statement

The Matlab script for picking fractures and a spreadsheet of fracture locations is available at PSU Scholarsphere https://www.doi.org/10.26207/4rvv-4c40.

Acknowledgments
This research used samples and/or data provided by the International Ocean Discovery Program (IODP). HMS was supported by an award from the U.S. Science Support Program/International Discovery Program (NSF-OCE 1450528). SS was supported by a Schlanger Ocean Drilling Fellowship. AF has received funding from the European Research Council (ERC) Horizon 2020 programme (grant agreement 715836). Rob Skarbek provided helpful comments on an early draft of the paper. The manuscript was greatly improved by a review from Zoe Shipton.

References

Ampuero, J. P., & Mao, X. (2017). Upper limit on damage zone thickness controlled by seismogenic depth. *Fault zone dynamic processes: Evolution of fault properties during seismic rupture* (Vol. 227, No. 243, pp. 10–1002).

Andrews, D. J., & Ben-Zion, Y. (1997). Wrinkle-like slip pulse on a fault between different materials. *Journal of Geophysical Research*, *102*(B1), 553–571. https://doi.org/10.1029/96jb02856

Barker, D. H., Henrys, S., Caratori Tontini, F., Barnes, P. M., Bassett, D., Todd, E., & Wallace, L. (2018). Geophysical constraints on the relationship between seamount subduction, slow slip, and tremor at the north Hikurangi subduction zone, New Zealand. *Geophysical Research Letters*, *45*(23), 12804–12813. https://doi.org/10.1029/2018gl080259

Barnes, P. M., Wallace, L. M., Saffer, D. M., Bell, R. E., B Underwood, M., Fagereng, A., et al. (2020). Slow slip source characterized by lithological and geometric heterogeneity. *Science Advances*, *6*(13), eaay3314. https://doi.org/10.1126/sciadv.aay3314

Bell, R., Holden, C., Power, W., Wang, X., & Downes, G. (2014). Hikurangi margin tsunami earthquake generated by slow seismic rupture over a subducted seamount. *Earth and Planetary Science Letters*, *397*, 1–9. https://doi.org/10.1016/j.epsl.2014.04.005

Bhat, H. S., Biegel, R. L., Rosakis, A. J., & Sammis, C. G. (2010). The effect of asymmetric damage on dynamic shear rupture propagation II: With mismatch in bulk elasticity. *Tectonophysics*, *493*(3–4), 263–271. https://doi.org/10.1016/j.tecto.2010.03.016

Blake, O. O., & Faulkner, D. R. (2016). The effect of fracture density and stress state on the static and dynamic bulk moduli of Westerly granite. *Journal of Geophysical Research: Solid Earth*, *121*(4), 2382–2399. https://doi.org/10.1002/2015JB012310

Brune, J. N. (2001). Shattered rock and precarious rock evidence for strong asymmetry in ground motions during thrust faulting. *Bulletin of the Seismological Society of America*, *91*(3), 441–447. https://doi.org/10.1785/0120000118

Caine, J. S., Evans, J. P., & Forster, C. B. (1996). Fault zone architecture and permeability structure. *Geology*, *24*(11), 1025–1028. https://doi.org/10.1130/0091-7613(1996)024<1025:fzaaps>2.3.co;2

Chester, F. M., & Logan, J. M. (1986). Implications for mechanical properties of brittle faults from observations of the Punchbowl fault zone, California. *Pure and Applied Geophysics*, *124*, 79–106. https://doi.org/10.1007/bf00875720

Cochran, E. S., Li, Y.-G., Shearer, P. M., Barbot, S., Fialko, Y., & Vidale, J. E. (2009). Seismic and geodetic evidence for extensive, long-lived fault damage zones. *Geology*, *37*(4), 315–318. https://doi.org/10.1130/g25306a.1

Coffey, G. L., Savage, H. M., Polissar, P. J., Meneghini, F., Ikari, M. J., Fagereng, A., et al. (2021). Evidence of seismic slip on a large splay fault in the Hikurangi subduction zone. *Geochemistry, Geophysics, Geosystems*.

Cook, A. E., Paganoni, M., Clennell, M. B., McNamara, D. D., Nole, M., Wang, X., et al. (2020). Physical properties and gas hydrate at a near-seafloor thrust fault, Hikurangi Margin, New Zealand. *Geophysical Research Letters*, *47*(16), e2020GL088474. https://doi.org/10.1029/2020GL088474

DeDontney, N., Templeton-Barrett, E. L., Rice, J. R., & Dmowska, R. (2011). Influence of plastic deformation on bimaterial fault rupture directivity. *Journal of Geophysical Research*, *116*(B10). https://doi.org/10.1029/2011jb008417

Duan, B. (2008). Asymmetric off-fault damage generated by bilateral ruptures along a bimaterial interface. *Geophysical Research Letters*, *35*(14). https://doi.org/10.1029/2008gl034797

El Mountassir, G., Lunn, R. J., Moir, H., & MacLachlan, E. (2014). Hydrodynamic coupling in microbially mediated fracture mineralization: Formation of self-organized groundwater flow channels. *Water Resources Research*, *50*, 1–16. https://doi.org/10.1002/2013WR013578

Fagereng, Å., Savage, H., Morgan, J., Wang, M., Meneghini, F., Barnes, P., et al. (2019). Mixed deformation styles observed on a shallow subduction thrust, Hikurangi margin, New Zealand. *Geology*, *47*(9), 872–876. https://doi.org/10.1130/g46367.1

French, M. E., & Morgan, J. K. (2020). Pore fluid pressures and strength contrasts maintain frontal fault activity, Northern Hikurangi Margin, New Zealand. *Geophysical Research Letters*, *47*(21), e2020GL089209. https://doi.org/10.1029/2020gl089209

Hamahashi, M., Saito, S., Kimura, G., Yamaguchi, A., Fukuchi, R., Kameda, J., et al. (2013). Contrasts in physical properties between the hanging wall and footwall of an exhumed seismogenic megasplay fault in a subduction zone—An example from the Nobeoka Thrust Drilling Project. *Geochemistry, Geophysics, Geosystems*, *14*(12), 5354–5370. https://doi.org/10.1002/2013gc004818

Heermance, R., Shipton, Z. K., & Evans, J. P. (2003). Fault structure control on fault slip and ground motion during the 1999 rupture of the Chelungpu fault, Taiwan. *Bulletin of the Seismological Society of America*, *93*(3), 1034–1050. https://doi.org/10.1785/0120010230

Ju, W., Hou, G., & Zhang, B. (2014). Insights into the damage zones in fault-bend folds from geomechanical models and field data. *Tectonophysics*, *610*, 182–194. https://doi.org/10.1016/j.tecto.2013.11.022

Kanamori, H., & Kikuchi, M. (1993). The 1992 Nicaragua earthquake: A slow tsunami earthquake associated with subducted sediments. *Nature*, *361*(6414), 714–716. https://doi.org/10.1038/361714a0

Keren, T. T., & Kirkpatrick, J. D. (2016). The damage is done: Low fault friction recorded in the damage zone of the shallow Japan Trench décollement. *Journal of Geophysical Research: Solid Earth*, *121*(5), 3804–3824. https://doi.org/10.1002/2015jb012311

Kristensen, T. B., Rotevatn, A., Peacock, D. C., Henstra, G. A., Midtkandal, I., & Grundvåg, S. A. (2016). Structure and flow properties of syn-rift border faults: The interplay between fault damage and fault-related chemical alteration (Dombjerg Fault, Wollaston Forland, NE Greenland). *Journal of Structural Geology*, *92*, 99–115. https://doi.org/10.1016/j.jsg.2016.09.012

Li, Y., Hou, G., Hari, K. R., Neng, Y., Lei, G., Tang, Y., et al. (2018). The model of fracture development in the faulted folds: The role of folding and faulting. *Marine and Petroleum Geology*, *89*, 243–251. https://doi.org/10.1016/j.marpetgeo.2017.05.025

Li, Y.-G., Chester, F. M., & Vidale, J. E. (2001). Shallow seismic profiling of the exhumed Punchbowl fault zone, Southern California. *Bulletin of the Seismological Society of America*, *91*(6), 1820–1830. https://doi.org/10.1785/0120000050

Ma, S., & Beroza, G. C. (2008). Rupture dynamics on a bimaterial interface for dipping faults. *Bulletin of the Seismological Society of America*, *98*(4), 1642–1658. https://doi.org/10.1785/0120070201

McKay, L., Lunn, R. J., Shipton, Z. K., Pytharouli, S., & Roberts, J. J. (2021). Do intraplate and plate boundary fault systems evolve in a similar way with repeated slip events? *Earth and Planetary Science Letters*, *559*, 116757. https://doi.org/10.1016/j.epsl.2021.116757

McNamara, D. D., Behboudi, E., Wallace, L., Saffer, D., Cook, A. E., Fagereng, A., et al. (2021). Variable in situ stress orientations across the northern Hikurangi subduction margin. *Geophysical Research Letters*, *48*(5), e2020GL091707. https://doi.org/10.1029/2020gl091707

McNeill, L., Ienaga, M., Tobin, H., Saito, S., Goldberg, D., Moore, J., & Mikada, H. (2004). Deformation and in situ stress in the Nankai Accretionary Prism from resistivity-at-bit images, ODP Leg 196. *Geophysical Research Letters*, *31*(2). https://doi.org/10.1029/2003gl018799

Mitchell, T., Ben-Zion, Y., & Shimamoto, T. (2011). Pulverized fault rocks and damage asymmetry along the Arima-Takatsuki Tectonic Line, Japan. *Earth and Planetary Science Letters*, *308*(3–4), 284–297. https://doi.org/10.1016/j.epsl.2011.04.023

Mitchell, T. M., & Faulkner, D. R. (2008). Experimental measurements of permeability evolution during triaxial compression of initially intact crystalline rocks and implications for fluid flow in fault zones. *Journal of Geophysical Research*, *113*(B11), B11412. https://doi.org/10.1029/2008jb005588

Mitchell, T. M., & Faulkner, D. R. (2009). The nature and origin of off-fault damage surrounding strike-slip fault zones with a wide range of displacements: A field study from the Atacama fault system, northern Chile. *Journal of Structural Geology*, *31*(8), 802–816. https://doi.org/10.1016/j.jsg.2009.05.002

Moore, J. C., & Saffer, D. (2001). Updip limit of the seismogenic zone beneath the accretionary prism of southwest Japan: An effect of diagenetic to low-grade metamorphic processes and increasing effective stress. *Geology*, *29*(2), 183–186. https://doi.org/10.1130/0091-7613(2001)029<0183:ulotsz>2.0.co;2

Morgan, J. K., Ramsey, E. B., & Ask, M. V. (2007). Deformation and mechanical strength of sediments at the Nankai subduction zone. *The seismogenic zone of subduction thrust faults* (pp. 210–256). Columbia University Press. https://doi.org/10.7312/dixo13866-008

Rabinowitz, H. S., Polissar, P. J., & Savage, H. M. (2017). Reaction kinetics of alkenone and *n*-alkane thermal alteration at seismic timescales. *Geochemistry, Geophysics, Geosystems*, *18*(1), 204–219. https://doi.org/10.1002/2016gc006553

Rowe, C. D., Meneghini, F., & Moore, J. C. (2009). Fluid-rich damage zone of an ancient out-of-sequence thrust, Kodiak Islands, Alaska. *Tectonics*, *28*(1). https://doi.org/10.1029/2007tc002126

Rowe, C. D., Moore, J. C., Remitti, F., & Scientists, I. E. T. (2013). The thickness of subduction plate boundary faults from the seafloor into the seismogenic zone. *Geology*, *41*(9), 991–994. https://doi.org/10.1130/g34556.1

Saffer, D. M. (2015). The permeability of active subduction plate boundary faults. *Geofluids*, *15*(1–2), 193–215. https://doi.org/10.1111/gfl.12103

Saffer, D. M., Wallace, L. M., Barnes, P. M., Pecher, I. A., Petronotis, K. E., LeVay, L. J., et al. (2019). Site U1518. In L. M. Wallace, D. M. Saffer, P. M. Barnes, I. A. Pecher, K. E. Petronotis, L. J. LeVay, & the Expedition 372/375 Scientists (Eds.), *Hikurangi subduction margin coring, logging, and observatories. Proceedings of the International Ocean Discovery Program* (Vol. 372B/375). International Ocean Discovery Program. https://doi.org/10.14379/iodp.proc.372B375.103.2019

Savage, H. M., & Brodsky, E. E. (2011). Collateral damage: Evolution with displacement of fracture distribution and secondary fault strands in fault damage zones. *Journal of Geophysical Research*, *116*(B3), B03405. https://doi.org/10.1029/2010jb007665

Savage, H. M., & Cooke, M. L. (2010). Unlocking the effects of friction on fault damage zones. *Journal of Structural Geology*, *32*(11), 1732–1741. https://doi.org/10.1016/j.jsg.2009.08.014

Savage, H. M., Keranen, K. M., Schaff, D. P., & Dieck, C. (2017). Possible precursory signals in damage zone foreshocks. *Geophysical Research Letters*, *44*(11), 5411–5417. https://doi.org/10.1002/2017GL073226

Savage, H. M., Rabinowitz, H. S., Spagnuolo, E., Aretusini, S., Polissar, P. J., & Di Toro, G. (2018). Biomarker thermal maturity experiments at earthquake slip rates. *Earth and Planetary Science Letters*, *502*, 253–261. https://doi.org/10.1016/j.epsl.2018.08.038

Savage, H. M., Shackleton, J. R., Cooke, M. L., & Riedel, J. J. (2010). Insights into fold growth using fold-related joint patterns and mechanical stratigraphy. *Journal of Structural Geology*, *32*(10), 1466–1475. https://doi.org/10.1016/j.jsg.2010.09.004

Shaddox, H. R., & Schwartz, S. Y. (2019). Subducted seamount diverts shallow slow slip to the forearc of the northern Hikurangi subduction zone, New Zealand. *Geology*, *47*(5), 415–418. https://doi.org/10.1130/g45810.1

Skelton, A., Claesson Liljedahl, L., Wästeby, N., Andrén, M., Tollefsen, E., Gudrunardottir, H. R., et al. (2014). Changes in groundwater chemistry before two consecutive earthquakes in Iceland. *Nature Geoscience*, *7*(10), 752–756. https://doi.org/10.1038/ngeo2250

Tavani, S., Storti, F., Lacombe, O., Corradetti, A., Muñoz, J. A., & Mazzoli, S. (2015). A review of deformation pattern templates in foreland basin systems and fold-and-thrust belts: Implications for the state of stress in the frontal regions of thrust wedges. *Earth-Science Reviews*, *141*, 82–104. https://doi.org/10.1016/j.earscirev.2014.11.013

Templeton, E. L., & Rice, J. R. (2008). Off-fault plasticity and earthquake rupture dynamics: 1. Dry materials or neglect of fluid pressure changes. *Journal of Geophysical Research*, *113*(B9). https://doi.org/10.1029/2007jb005529

Tobin, H., Vannucchi, P., & Meschede, M. (2001). Structure, inferred mechanical properties, and implications for fluid transport in the décollement zone, Costa Rica convergent margin. *Geology*, *29*(10), 907–910. https://doi.org/10.1130/0091-7613(2001)029<0907:simpai>2.0.co;2

Todd, E. K., Schwartz, S. Y., Mochizuki, K., Wallace, L. M., Sheehan, A. F., Webb, S. C., et al. (2018). Earthquakes and tremor linked to seamount subduction during shallow slow slip at the Hikurangi margin, New Zealand. *Journal of Geophysical Research: Solid Earth*, *123*(8), 6769–6783. https://doi.org/10.1029/2018jb016136

Vermilye, J. M., & Scholz, C. H. (1998). The process zone: A microstructural view of fault growth. *Journal of Geophysical Research: Solid Earth*, *103*(B6), 12223–12237. https://doi.org/10.1029/98jb00957

Viesca, R. C., Templeton, E. L., & Rice, J. R. (2008). Off-fault plasticity and earthquake rupture dynamics: 2. Effects of fluid saturation. *Journal of Geophysical Research: Solid Earth*, *113*(B9). https://doi.org/10.1029/2007jb005530

Wallace, L. M., Beavan, J., McCaffrey, R., & Darby, D. (2004). Subduction zone coupling and tectonic block rotations in the North Island, New Zealand. *Journal of Geophysical Research*, *109*(B12). https://doi.org/10.1029/2004jb003241

Wallace, L. M., Saffer, D. M., Barnes, P. M., Pecher, I. A., Petronotis, K. E., LeVay, L. J., & Expedition 372/375 Scientists. (2019). Hikurangi subduction margin coring, logging, and observatories. Proceedings of the International Ocean Discovery Program (Vol. 372B/375). International Ocean Discovery Program.

Wallace, L. M., Webb, S. C., Ito, Y., Mochizuki, K., Hino, R., Henrys, S., et al. (2016). Slow slip near the trench at the Hikurangi subduction zone, New Zealand. *Science*, *352*(6286), 701–704. https://doi.org/10.1126/science.aaf2349

Williams, J. N., Toy, V. G., Massiot, C., McNamara, D. D., & Wang, T. (2016). Damaged beyond repair? Characterising the damage zone of a fault late in its interseismic cycle, the Alpine Fault, New Zealand. *Journal of Structural Geology*, *90*, 76–94. https://doi.org/10.1016/j.jsg.2016.07.006